OPTIMIZATION OF SELECTIVE LASER SINTERING PROCESS FOR FABRICATION OF ZIRCONIUM DIBORIDE PARTS

Ming C. Leu[1], Shashwatashish Pattnaik[1], Gregory E. Hilmas[2]
[1]Department of Mechanical and Aerospace Engineering, Missouri University of Science and Technology, Rolla, Missouri, USA
[2]Department of Materials Science, Missouri University of Science and Technology, Rolla, Missouri, USA

Abstract

Selective Laser Sintering (SLS) was investigated to fabricate Zirconium Diboride (ZrB_2) parts for ultra-high temperature applications. Experiments were conducted to determine values of SLS process parameters (laser power, scan speed, line spacing, and layer thickness) that can be used to build ZrB_2 parts with high integrity and sharp geometrical features. A sacrificial plate with a proper number of layers (determined from experimentation) separated from the main part was built in order to reduce thermal gradients when building the main part. The sacrificial plate was found to assist in eliminating cracks in the bottom of the main part. The fabricated green parts then went through post processing steps including binder burnout and sintering at proper temperature schedules, to remove the binder and sinter the ZrB_2 particles. The test bars after sintering had an average relative density of 87% and an average flexural strength of 250 MPa.

1. Introduction

Fabrication of geometrically complex ceramic parts is difficult using traditional manufacturing techniques. This is due to the extremely brittle nature of ceramics. The high cost involved in machining of ceramics due to material wastage is another reason that reduces the desirability of using material removal methods for fabrication of complex ceramic parts.

Many Solid Freeform Fabrication (SFF) methods have been used in attempt to fabricate ceramic parts. Among these are the Fused Deposition of Ceramics (FDC) [1,2], Chemical Liquid Deposition (CLD) [3], Selective Laser Melting (SLM) [4], Shape Deposition Manufacturing (SDM) [5,6], 3D Printing (3DP) [7], Stereolithography (SLA) [8-10], Laminated Object Manufacturing (LOM) [11,12] and Selective Laser Sintering (SLS) [13,14]. Although these methods have been successfully implemented for freeform fabrication of ceramic parts, each has limitations on its own. Limited materials available for some of the processes, inability to fabricate complex geometries, long duration to fabricate parts and difficulties in process control are the major challenges that need to be overcome.

Selective Laser Sintering of ZrB_2 has previously been attempted by Stucker's research team [15,16]. The part obtained after that SLS processing was of preliminary shape and needed to be machined after debinding and sintering to obtain accurate shape. The debinded and sintered SLS-produced ZrB_2 samples had only 31% in relative density. The SLS-produced ZrB_2 parts were then infiltrated with Cu to make EDM electrodes. Another study was reported to have successfully sintered ZrB_2 part using a combination of a continuous wave and pulsed laser [17]. This study did not use any binder material.

Instead, smaller ZrB_2 particles melted to act as a binder for larger ZrB_2 particles. There was no report of any mechanical properties or evidence of successful fabrication of geometrically complex parts.

The present paper describes an empirical study to investigate a technique for fabricating 3-dimensional ZrB_2 parts using the SLS process and to determine optimal values of SLS process parameters. The flexural strength and density of the fabricated parts after binder burnout and sintering were measured and evaluated.

2. Effects of process parameters and heat transfer

2.1 *Process parameters*

2.1.1 *Part bed temperature*

The part bed is the central region of the SLS machine (DTM Sinterstation 2000) where the part is built. The part bed temperature is controlled primarily by the heater underneath the build area. The norm is to set the temperature slightly below the melting temperature of the binder material, which melts to fuse the ceramic particles [18]. The higher the temperature is set, the less the incident energy is required during the SLS process. This also lowers the temperature gradient between the part being built and its surrounding powder, thereby reducing part distortion [19]. However, the binder will become sticky and clump the ceramic particles together if the temperature is set too high.

2.1.2 Layer thickness

Layer thickness is a measure of the thickness of each layer during the SLS process. It is also the depth by which the part piston is lowered after the laser scanning of each layer. A stair-step effect has been observed [20] which affects the surface finish of the side face of a fabricated part. Layer thickness plays an important role in determining the appropriate set of laser parameters, as a thicker layer requires greater incident energy to avoid delamination in fusing subsequent layers. Layer thickness also plays an important role in determining the total build time.

2.1.3 Energy density

Energy density is defined as the amount of energy input per unit area. It is dependent upon laser power, scan speed and scan spacing and is determined by the following equation [21]:

$$ED = LP / (BS \text{ x } SS) \ldots\ldots\ldots\ldots\ldots\ldots\ldots\ldots\ldots\ldots\ldots\ldots\ldots\ldots\ldots\ldots\ldots\ldots\ldots.. (1)$$

where ED is the energy density, LP is the laser power, BS is the beam scan speed and SS is the scan spacing. The laser power, scan speed and scan spacing need to be optimized according to the amount of input energy required to fuse the particles in the layer.

2.1.4 Effects on green part strength

The set of parameters used to fabricate a part plays a major role in influencing the green part strength. Previous research has shown that the binder content and the energy density significantly affect the part strength [18, 22]. Higher binder content has been shown to improve the green part strength, but leads to greater shrinkage of the part in the post processing owing to the pyrolysis of a greater amount of the binder. The other important factor that affects the part strength is the incident energy density. It has been

reported that the strength of a green part increases with increase in energy density and peaks at a certain value [18]. The decrease in strength beyond the peak energy density is due to more polymer degradation at higher energy densities. The SLS parameters need to be optimized keeping these relationships in mind.

2.2 Heat transfer

Since SLS is a process where the part creation revolves around heat transfer, most problems are associated with the amount of heat input and the rate of heat transfer. As the heat is applied on the top surface, the binder on the top surface melts and solidifies, resulting in contraction of the top surface and thus a change in powder density. The resultant temperature gradient perpendicular to the layered surface causes a problem of upward warping of the layer. This often results in cracking of the layer when the next layer of powder is spread and compressed by the roller. Some approaches have been taken to solve this problem [19]. In the case of metal or polymer powder, raising the part bed temperature to near the melting point of the part material can result in a reduction of temperature gradients and solve the problem of upward warping in some cases [23].

An approach introduced in the current research is the use of a sacrificial plate built from the same material as the part itself. An appropriate number of separation layers is needed so as to avoid binding the part to the sacrificial plate. The sacrificial plate would provide better conduction of heat during laser scanning for fabricating the main part. A previous study [24] of conductivity of sintered powder compacts helps explain the phenomenon. This study reported that the effective thermal conductivity, G_e, of a powder compact can be calculated using the following equation:

$$G_e = G_o \, (1\text{-}\emptyset/\, \emptyset_M)^2 \dots\dots\dots\dots\dots\dots\dots\dots\dots\dots\dots\dots\dots\dots\dots\dots\dots\dots\dots\dots. (2)$$

where G_o is the thermal conductivity of the monolithic material, $\emptyset$ is the compact porosity and $\emptyset_M$ is the tap porosity. The tap porosity is the porosity of particle aggregate in equilibrium after vibratory mixing (but without compaction). It is dependent on the particle shape, size and distribution. As the tap porosity is a constant for the same particle shape, size and distribution, the effective conductivity is mainly dependent on the compact porosity, which is the porosity of the powder after compaction. A sacrificial plate effectively reduces the compact porosity of the layers underneath the main structure, thus resulting in better heat conduction.

3. Materials and Methods

3.1. Materials used

The materials used for this investigation included zirconium diboride (ZrB_2, grade B, H.C. Starck, Newton, MA) with an average particle size of 3μm. The organic binder used was stearic acid ($C_{18}H_{36}O_2$, grade HS, Acros Organics, New Jersey), which was chosen due to its ability to easily depolymerize at higher temperatures, leaving little or no carbon residue. Two sintering additives used were boron carbide (B_4C, grade HS, H.C. Stark, Newton, MA) and carbon black (Black Pearls 120, Cabot corporation, Alpharetta, GA). The sintering additives assisted in removal of the oxides from the surface of the ZrB_2 powder and increased the driving force for densification instead of grain growth.

3.2. Powder preparation

Homogeneous mixing of the powder contents including ZrB_2, stearic acid, boron carbide (1 wt%) and carbon black (0.2 wt%) was achieved through two steps. First, zirconium diboride, boron carbide and carbon black were ball-milled together using alumina media for a period of 24 hours. Then, stearic acid was added to the mix at a volumetric ratio of 50:50 and the mixture was ball-milled for another 24 hours. Regular inspections were carried out to check for possible clumping during the ball milling.

3.3. SLS processing

Test bars and fuel injector struts (small scale) as shown in Figure 2 were made by the SLS process to investigate the feasibility of fabricating ZrB_2 parts using this process. The test bars were first built for selection of process parameters. The temperatures considered were those of the feed bins, part bed and part heater.
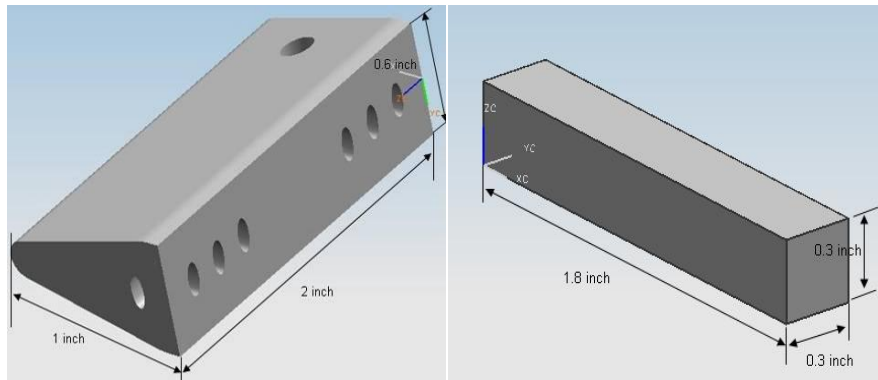

Figure 1 CAD models of fuel injector strut and test bar

The layer thickness was set at 0.0762 mm (0.003"), which is the lowest possible value that can be set in the Sinterstation 2000. This was done to attain the best surface finish and also to allow the molten binder to flow down to join the layers and help avoid delamination.

The part bed temperature was kept in the range of 55 to 60 ^{o}C, slightly below the melting point of stearic acid (69 ^{o}C). The feed bin temperature needs to be kept low enough to avoid having the binder clump (partial sintering) inside the bin, but the temperature also has to be high enough to assist in rapid heating of the powder. It was observed that good flowability of the powder was achieved at room temperature and hence both bins were set at 26 ^{o}C. The laser power, scan speed and scan spacing were set with the help of Equation (1).

The experiments performed in SLS processing consisted of the following 2 stages:

STAGE 1: This stage of tests consisted of 4 runs (Runs 1 to 4), which were carried out to determine the appropriate energy density at which green parts could be fabricated without delamination and were strong enough for subsequent handling. The energy densities tested were 0.068, 0.103, 0.115 and 0.172 J/mm^2 in these four runs. The corresponding parameter settings are given in Table 1.

STAGE 2: This stage of tests consisted of 3 runs (Runs 5 to 7), which were dedicated to addressing the issue of cracks in the bottom of the part. These 3 runs were

carried out based upon the observations from the runs in STAGE 1. The parameter settings and sacrificial plates used are also given in Table 1.

Table 1 Parameter settings for green part fabrication

RUN No.	Laser Power, W	Scan Speed, mm/s	Scan Spacing, mm	Energy Density, J/mm^2	No. of Separation Layers	Sacrificial Plate (cross-section size)
STAGE 1						
1	0.8	50.8	0.2286	0.068	n/a	n/a
2	1.2	50.8	0.2286	0.103	n/a	n/a
3	2	76.2	0.2286	0.115	n/a	n/a
4	3	76.2	0.2286	0.172	n/a	n/a
STAGE 2						
5	2	76.2	0.2286	0.115	5	Same as part size
6	40	1524.0	0.2286	0.115	5	Larger than part size
7	2	76.2	0.2286	0.115	3 to 8	Larger than part size

3.4. Post processing

After fabrication of green parts with the SLS machine, the successful test bars underwent binder burnout, cold isostatic pressing and sintering. Binder burnout was carried out in a Lindberg furnace of Type 51542-HR, where the parts were heated in varied increment rates to a temperature of 600 ^{o}C in an inert environment (90% Argon +10% Hydrogen) and held for approximately an hour to thermally decompose the binder. After the binder burnout the specimens underwent isostatic pressing at a pressure of 40,000 psi at room temperature. This was performed to reduce the porosity and the distance between particles to promote sintering in the next stage. The successful parts after the isostatic pressing underwent sintering in a furnace (Hi-temp furnace, Thermal Technology Inc, Santa Rosa, California) at a temperature of 2050 ^{o}C for 2 hours.

3.5. Evaluation

The successful test bars were used to study the dimensional accuracy, density, and flexural strength, and the microstructures were evaluated. The green and sintered densities were determined by measuring the dry, saturated and suspended weight using a weighing scale (Acculab, Sartorius Group, USA) based on the Archimedes principle using water as the immersing medium. The relative density of the samples was obtained with respect to the theoretical density of ZrB_2 (6.1 g/cm^3). The flexural strength of a fully sintered specimen was measured by a four-point bending flexural test using a universal testing machine (Instron Corp., Model No. 5581, Norwood, MA, USA). All samples were ground to standard A bar regulations (20 x 2 x 1.5) and polished in accordance to the ASTM C1161 standards [35].

The microstructures of the specimens were observed under a Scanning Electron Microscope (S-4700, Hitachi Corp, USA). Polished, unpolished and fractured surfaces were examined to distinguish and measure the closed and open porosity in the specimens.

4. Results and discussion

4.1. Selection of SLS parameters

The Stage 1 experiments were aimed at determining appropriate energy density for creating the melt pool. In the four runs (see Table 1), Run 3 produced parts of the highest quality. The parameter settings of Run 3 had an energy density of 0.115 J/mm^2, which was sufficient to melt the binder and create a melt pool that could flow through the layers and bind the ZrB_2 particles together. Parts fabricated in Run 3 demonstrated better green strength when compared to Run 1 and Run 2 and did not show any signs of delamination. Run 1 did not produce any usable green parts due to insufficient energy density. Run 2 produced parts of strength insufficient for proper handling, as only 17% of the parts survived the part breakout process without any breakage. Similar to Run 3, Run 4 was also able to produce strong parts that showed no delamination and no breakage during the part breakout process. However, parts from Run 4 had poorer quality on the bottom surface (more material loss due to cracks on the bottom surface) when compared with parts from Run 3. In all of the runs the initial layers warped after laser scanning, which caused cracking of the initial part layers. The cracks were deeper in the case of parts fabricated at the energy density of 0.172 J/mm^2 in Run 4 when compared with 0.115 J/mm^2 in Run 3. The deeper cracks caused more material loss from the part bottom when blown by air during the part cleaning process.

4.2. Elimination of bottom surface cracking

In all the four runs performed above, the bottom surface of the parts showed cracks. These cracks were caused by deformation in the initial layers, which warped upwards after laser scanning. The warped layer then cracked when the roller applied pressure on it while spreading a new layer of powder on top of the proceeding layer. These cracks would extend until about 10-15 layers of powder had been fabricated in the SLS process. Figure 2 shows warping of the second layers after laser scanning.

Figure 2 Warping of the 2nd layers after laser scanning

The warping problem was addressed by performing the following tests:
i)   A sacrificial plate (one for each part in the build) having the same X-Y dimensions as the part size was built underneath the part with 5 separation layers of loose powder between the part and the sacrificial plate. This was performed in Run 5, using the laser parameter settings developed in Run 3.
ii)   A sacrificial plate covering the entire build surface area was built underneath the parts with 5 separation layers of loose powder between them. This was performed in Run 6, where the laser parameter settings were changed to increase productivity. The scan speed and the laser power were each increased by a factor of 20, keeping the energy density same as in Run 3.
iii)   One sacrificial plate covering the entire build surface area was built underneath the parts with a separation ranging from 3 to 8 layers between the part and the sacrificial plate. This was performed in Run 7. The laser parameter settings were kept the same as those in Run 3.

The experimental observations indicated that the use of a small sacrificial plate having the same size as the built part (in Run 5) was not sufficient to solve the temperature gradient problem. It was unable to affect heat conduction enough to avoid warping, which results in cracking in the bottom of the built part.

The use of a larger sacrificial plate (in Run 6) helped in heat conduction through the part bed but because of great reduction in scan time between layers (due to high scan speed), the melt pool increased drastically and percolated through the separation layers of loose powder and fused the sacrificial plate and the main part together. Also due to the thermal stress developed in the part, cracks developed throughout the part.

The use of a larger sacrificial plate (in Run 7) with the laser parameters set as in Run 3 helped solve the issue of bottom layer cracking, and a part with sufficient green strength for handling and without any cracks could be successfully fabricated. The separation layers were also optimized by varying the number of separation layers in the range of 5 to 8. In the case of test bars, successful parts were fabricated with 7 and 8 layers of separation. In the case of injector struts, the successful parts were fabricated with 5 and 6 layers of separation. The difference in the separation layers for the test bars and the injector struts is due to the difference in the cross section of the initial layers. The successfully fabricated parts can be seen in Figures 3 and 4 for these two kinds of parts.
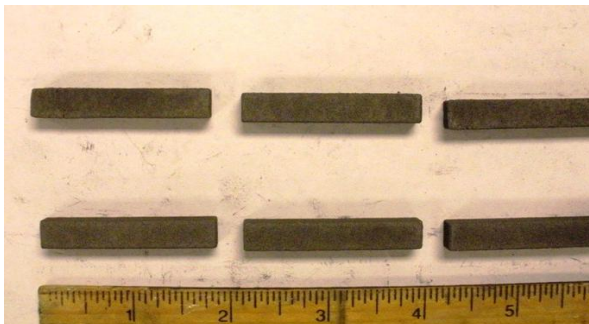

Figure 3 Successful green test bars   Figure 4 Successful green injector parts

Optimization of number of separation layers is important because a small number of separation layers would result in fusing of the main part with the sacrificial plate, whereas a large number of separation layers would result in a reduced effect of the sacrificial plate, causing cracks on the bottom surface of the main part.

The results of Run 6 and Run 7 show that the same energy density but different laser power and scan speed can produce very different results. At a scan speed of 50.8 mm/s the time interval between the two consecutive laser scans of 25.4 mm long is 0.5 seconds, while in case of 1,524 mm/s it is 0.017 seconds. In the case of Run 6, the scanned layer did not get enough time to cool down and solidify sufficiently before the spreading of the next layer of powder, thus each new layer was being deposited on a partially molten layer as was observed in the experiment. Hence the part deformed due to the lack of support by the previously scanned layer in fabricating a new layer. Also the rapid heating in Run 6 led to development of larger thermal stresses, which contribute to part deformation and cracking.

4.3. Evaluation of fabricated parts

After post-processing, the parts fabricated were evaluated for mechanical strength and density. The dimensions of the parts were measured after each stage to check for shrinkage. The microstructure of the parts was studied using SEM images.

The parts fabricated using energy density of 0.115 J/mm^2 demonstrated higher mechanical strength and density in comparison to the parts fabricated using energy density of 0.103 J/mm^2. The average shrinkage of parts fabricated using 0.115 J/mm^2 was significantly lower than those fabricated using 0.103 J/mm^2. The SEM images showed lower porosity and smaller pores in case of parts fabricated at 0.115 J/mm^2 as compared to 0.103 J/mm^2. These results show that high energy density helps bind the particles and layers and thus facilitates better sintering at later stage.

The dimensions of the successful parts fabricated were measured using Mitutoyo vernier calipers. The average dimensional reductions for sintered test bars, fabricated using energy density 0.103 J/mm^2 (Run 2) in the X, Y and Z directions were 19%, 21% and 41% of the nominal dimensions, respectively. The average reductions for fuel injector struts for the same settings in the X, Y and Z direction were 16%, 17% and 38% of the nominal dimensions, respectively. The dimensional changes in the X and Y directions are low as compared to that in the Z direction. This is because the lower energy density was unable to create a melt pool that could percolate downwards and sufficiently bind the particles between two layers.

The average dimensional reductions for test bars fabricated using energy density 0.115 J/mm^2 (Run 3) were 16%, 11% and 12% of the nominal dimension in the X, Y and Z direction, respectively. The average dimensional reductions in the fuel injector struts fabricated were 13%, 13% and 15% of the nominal dimension in the X, Y and Z directions, respectively. The higher energy density created a sufficiently large melt pool, allowing more molten binder to percolate through the layer to bind more particles together. This is the reason for the shrinkage in Z direction of parts fabricated in Run 3 being lower than the shrinkage resulted in Run 2.

The relative density for the sintered test bars was measured using the Archimedes method. The parts fabricated using energy density of 0.115 J/mm^2 had 87.1% in relative density compared to 80.3% for parts fabricated using 0.103 J/mm^2. This demonstrates

better fusion of ceramic particles at the higher energy density. The closer packing at the higher energy density resulted in lower porosity, which provides less room for shrinkage.

The test bars fabricated using 0.103 J/mm^2 had an average flexural strength of 195 MPa (ranging between 162 MPa to 246 MPa). The test bars fabricated using 0.115 J/mm^2 had an average flexural strength of 250 MPa (ranging between 212 MPa to 315 MPa).

The microstructures studied with SEM images show that the porosity is higher in parts fabricated at lower energy density settings. Figure 5 shows images of sample fractured surfaces of the test bars at energy density settings of 0.103 J/mm^2 and 0.115 J/mm^2. It can be observed that the grain structure has larger pores and higher porosity when ED = 0.103 J/mm^2 compared with ED = 0.115 J/mm^2. This is consistent with the observation that the density of the fabricated part at ED = 0.103 J/mm^2 is lower than that at ED = 0.115 J/mm^2.

(a)

(b)

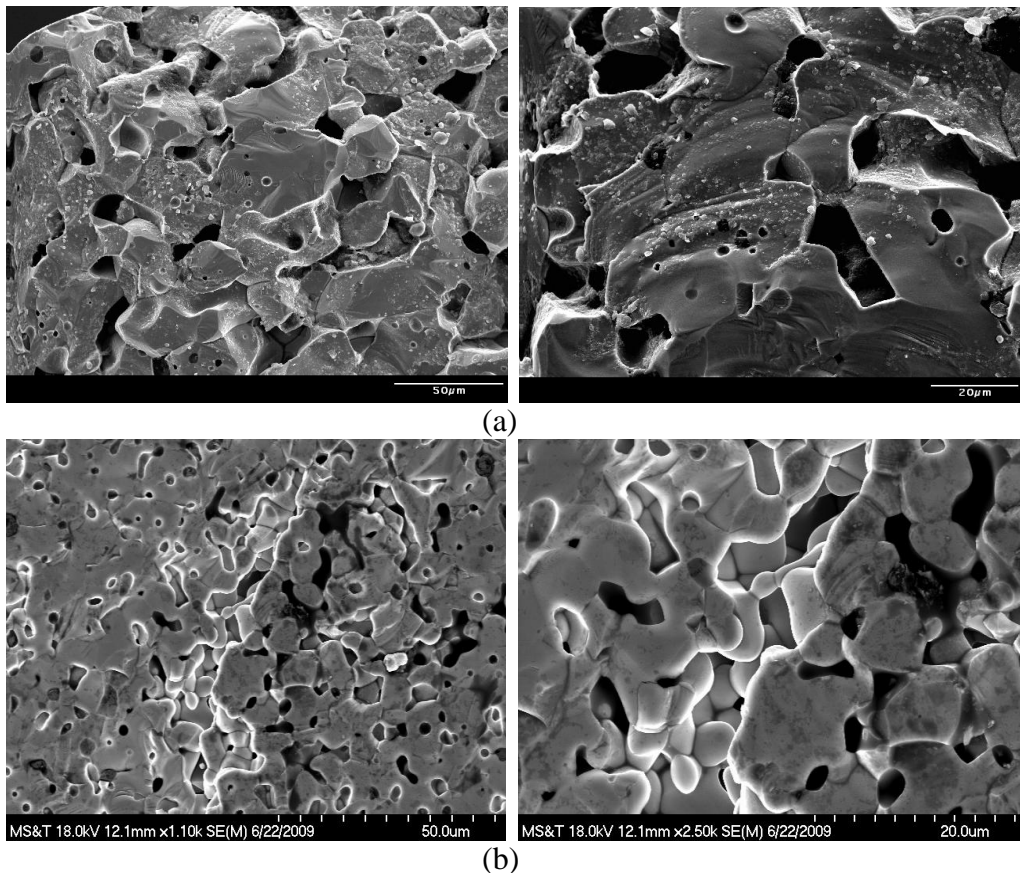Figure 5 SEM images of fractured surfaces of test bars fabricated at (a) ED = 0.103 J/mm^2 and (b) ED =0.115 J/mm^2

5. Conclusion

The proper parameter settings for laser power, scan speed and scan spacing were determined experimentally in the fabrication of ZrB$_2$ parts using the SLS process. The use of a sacrificial plate has been shown beneficial in eliminating cracks at the bottom of the part by facilitating more uniform heat conduction and hence reduction of thermal gradient. The number of separation layers between the sacrificial plate and the main part was experimentally determined to be in the range of 5 to 8 layers in the fabrication of test

bars and fuel injector struts. The average flexural strength of the test bars increased with increase in input energy density up to 0.115 J/mm^2. The average flexural strength achieved, at energy density of 0.115 J/mm^2, for the fabricated test bars after binder burnout and sintering was 250 MPa and the relative density achieved was 87%.

Acknowledgments

References
1. Jafari, M. A., Han, W., Mohammadi, F. and Safari, A., 2000. A novel system for fused deposition of advanced multiple ceramics. *Rapid Prototyping Journal*, 6 (3), 161-175.
2. Agarwala, M. K., Jamalabad, V. R., Langrana, N. A., Safari, A., Phillip, J. W. and Danforth, S. C., 1996. Structural quality of parts processed by fused deposition. *Rapid Prototyping Journal*, 2 (4), 4-9.
3. He, Z., Zhou, J.G. and Tseng, A.A., 2000. Feasibility study of chemical liquid deposition based solid freeform fabrication. *Materials and Design*, 21 (2), 83-92.
4. Tang, Y., Fuh, J.Y.H., Loh, H.T., Wong, Y.S. and Lu, L., 2003. Direct laser sintering of silica sand. *Materials and Design*, 24 (8) 623-629.
5. Cooper, A.G., Kang, S., Kietzman, J.W., Prinz, F.B., Lombardi, J.L. and Weiss, L. 1999. Automated fabrication of complex molded parts using mold SDM. *Materials and Design*, 20 (2) 83-89.
6. Kietzman, J.W., Cooper, A.G., Weiss, L.E., Schultz, L., Lombardi, J.L. and Prinz, F.B., 1997. Layered manufacturing material issues for SDM of polymers and ceramics. *Proceedings of Solid Freeform Fabrication symposium*, 133-140.
7. Sachs, M.E., Haggerty, J.S., Cima, M.J. and Williams, P.A., 1993. Three dimensional printing techniques. *United States Patent -5,204,055.*
8. Brady, A. G. and Halloran, J. W., 1997. Stereolithography of ceramic suspensions. *Rapid Prototyping Journal*, 3 (2), 61-62.
9. Doreau, F., Chaput, C. and Chartier, T., 2000. Stereolithography for manufacturing ceramic parts. *Advanced Engineering Materials*, 2 (8), 493-496.
10. Doreau, F., Chaput, C., Chartier, T. and Loiseau, M., 2002. Stereolithography of structural complex ceramic parts. *Journal of Materials Science*, 37 (15), 3141-3147.
11. Klosterman, D.A., Chartoff, R.P., Osborne, N.R., Graves, G.A., Lightman, A., Han, G., Bezeredi, A. and Rodrigues, S., 1999. Development of a curved layer LOM process for monolithic ceramics and ceramic matrix composites. *Rapid Prototyping Journal*, 5 (2), 61-71.
12. Zhang, Y., He, X., Du, S. and Zhang, J., 2001. Al$_2$O$_3$ ceramics preparation by laminated object manufacturing. *The International Journal of Advanced Manufacturing Technology*, 17 (7), 531-534.

13. Bourell, D.L., Marcus, H., Barlow, J. and Beaman, J.J., 1992. Selective laser sintering of metals and ceramics. *International Journal of Powder Metallurgy*, 28 (4), 369-381.
14. Liu, Z.H., Nolte, J.J., Packard, J.I., Hilmas, G., Dogan, F. and Leu, M.C., 2007. Selective laser sintering of high-density alumina ceramic parts. *Proceedings of the 35th International MATADOR conference*, 351-354.
15. Stucker, B.E., Bradley, W.L., Eubank, P.T., Bozkurt, B. and Norasethekkul, S., 1999. Manufacture and use of ZrB_2 /Cu or TiB_2 /Cu composite electrodes. *United States Patent – 5,933,701.*
16. Stucker, B.E., 1997. Rapid prototyping of zirconium diboride/copper EDM electrodes. Dissertation (PhD), Texas A&M University.
17. Sun, N.C. and Gupta, M.C., 2008. Laser sintering of ZrB_2. *Journal of American Ceramic Society*, 91 (5), 1729-1731.
18. Agarwala, M., Bourell, D.L., Beaman, J.J., Marcus, H. and Barlow, J., 1995. Direct selective laser sintering of metals. *Rapid Prototyping Journal*, 1 (1), 26-36.
19. Pham, D.T., Dimov, S. and Lacan, F., 1999. Selective laser sintering: applications and technological capabilities. *Proceedings of the Institution of Mechanical Engineers, Part B: Journal of Engineering Manufacture*, 213 (5), 435-449.
20. Gibson, I. and Shi, D., 1997. Material properties and fabrication parameters in selective laser sintering process. *Rapid Prototyping Journal*, 3 (4), 129-136.
21. Nelson, J.C., 1993. Selective Laser Sintering: A definition of the process and an empirical sintering model. Dissertation (PhD), University of Texas, Austin.
22. Badrinarayan, B. and Barlow, J.W., 1990. Effect of processing parameters in SLS of metal-polymer powders. *Proceedings of the Solid Freeform Fabrication, Austin, Texas*, 55-63.
23. Williams, J.M., Hysinger, C. and Beaman, J.J., 1992. Design of a high temperature process chamber for the selective laser sintering process. *Proceedings of the Solid Freeform Fabrication, Austin, Texas*, 110-117.
24. Montes, J.M., Rodriguez, J.A. and Herrera, E.J., 2003. Thermal and electrical conductivities of sintered powder compacts. *Powder Metallurgy*, 46 (3), 251-256.
25. ASTM International, 2008, Standard test method for flexural strength of advanced ceramics at ambient temperature, ASTM C1161-02c, West Conshohocken, Pennsylvania, USA.